Indian Journal of Engineering & Materials Sciences
Vol. 33, February 2026, pp. 87-92
DOI: 10.56042/ijems.v33i01.22728

Structural properties and porous nature of newly developed NEG materials

Surendra kanikella[a]*, Kanni pamula Vijaya Babu[a], Ampolu Satheesh[b], Elayaperumal Sumitha[c] & Angagalakuduru Durga Prasada Rao[d]

[a] Department of Physics, Centurion University of management and Technology, Vizianagaram 535 003, Andhra Pradesh, India

[b]Department of Chemistry, Centurion University of management and Technology, Vizianagaram 535 003, Andhra Pradesh, India

[c]Department of Biotechnology and Bioinformatics, JSSAHER, Mysore 570 015, Karnataka, India

[d] Department of Nuclear Physics, Andhra University Visakhapatnam 530 003, Andhra Pradesh, India

Received: 14 August 2025; accepted: 17 December 2025

Non-Evaporable Getter (NEG) applications have increased significantly in recent years, and these materials have been widely used at high temperatures for various applications. The present study has discussed the structural properties and porosity nature of newly developed getter materials with rare earth (RE-Samarium and Gadolinium) element substitutions. The selected materials, namely Zr–Co and Zr–Co–(Sm+Gd) with different compositions, have been synthesized using the solid-state reaction method, and the alloys have been activated at a temperature of 1000°C. The obtained results have been analyzed using X-ray Diffraction (XRD) for structural analysis, Scanning Electron Microscopy (SEM) coupled with Energy Dispersive Spectroscopy (EDS) for morphological and elemental analysis, and Transmission Electron Microscopy (TEM) for microstructural evaluation and particle size determination. Furthermore, Thermogravimetric Analysis (TGA) and Differential Scanning Calorimetry (DSC) have been employed to explain the nitrogen storage capacity of the NEG materials. The present work has aimed to study and compare the structural parameters and porosity nature of pure and rare-earth substituted NEG alloys.

Keywords: Activation temperature, Porosity, Structural properties, Zr-Co, Zr-Co-RE NEG materials

1 Introduction

The getters are expected to have maximized surface to volume ratios with high porosity facilitating to access the gas to be pumped to the internal areas of the getter. The combination of these four series of materials is assumed to provide good mechanical characteristics facilitating them to be the suitable getters for required conditions[1-3]. A simple and reliable method for determining the porosity of a solid sample is adopted in the present study that involves use of its lattice constant value. In the past few years, many NEG alloys have been used for different applications in vacuum technology. For these reasons, the Zr-V-Ti, Zr-V-Fe, Zr-Al, and Zr-Co non-evaporable getter alloys were widely used to achieve better vacuum-type devices[4,5]. Also, these support chemical reactions of getter and gases to maintain good vacuum conditions in the machines. The primary need for non-evaporable getter materials is high activation temperature, high resolvability limitation and high conductivity to the absorbed categories, high temperature and high chemical strength[6]. The NEG materials with the high activation temperature are Zr-Coalloys. Therefore, NEG materials are essential for obtaining and maintaining vacuum conditions for ultra-high or extremely ultra-high vacuum systems. This paper discussed the structural properties, morphologies, microstructure, and porosity nature performance of substituting rare-earth elements Sm and Gd of NEG getter materials[7-10].

2 Materials and Methods

The composition of the NEG getter alloys is derived from stoichiometry ratios starting with Zr, and Co metal powders from Sigma Aldrich (99.99%) and rare-earth (RE) components Samarium and Gadolinium metal powders from Merck (99.99%). The chemical compositions Zr_{1-x}+Co_x and Zr_{1-x} Co_{x-3}-$(Sm+Gd)_3$ are synthesized, where x=0, 40, 80, 120in steps. The mixed raw powder material was first thoroughly milled for 15 hours using an agate mortar and pestle to add methanol solvent to bind the substance. This combined powder material was heated

*Corresponding author: (E-mail: keth.surendra@gmail.com)

in a muffle box furnace for 1 hour at 350°C to remove the moisture content in the metal powder. When the heated powder material has cooled to its normal temperature, it is grinding again for one hour to make the materials well blended. The powder material to make into pellets in round discs using a KBr Hydraulic Pellet Presser with a pressure of 3 tonnes for 5 minutes on the pellet machine to generate NEG alloys. These are sintered in a muffle furnace at 1000°C for 2 hours to make non-evaporable getter alloys. The XRD patterns of both series of materials were obtained using a Panalytical X-pert pro-diffract-meter with diffraction angles ranging from 10° to 80°in 0.02° steps. A transmission electron microscope (TEM) made by the Philips Company, a scanning electron microscope (SEM), and an energy dispersive spectrometer (EDS) made by JEOL were used to look at the materials' shapes and how they were made.

3 Results and Discussion

3.1 X-ray diffraction studies

The XRD technique is a universally accepted method to determine the behavior of the crystal and its structure. The material is basically in the form of powder, comprising fine particles of material with a single crystalline to be studied. This technique is extensively utilized for structure analysis, structure determination, crystallite size, lattice constant, texture and electron radial distribution functions. The XRD analysis for the synthesized getter material is carried out to study the relation between crystallographic properties and their variation with rare earth elements substitution. The lattice constant and XRD patterns measure the cell volume of each sample to assess the influence of RE element replacements on the crystalline lattice of the better-getter materials developed. In Fig. 1 Zr $_{1-x}$-Co_x series exhibitssix fingerprint peaks at h k l values (1 0 0), (1 1 0), (1 1 1), (2 0 0), (2 1 0), and (2 1 1) tare matches with JCPDS Card No #00-018-0436[11, 12]. The acquired Zr-Co_2 phase also exhibits cubic structure and reflects very low intense diffraction peaks corresponding to (2 2 0), (4 0 0) and (4 4 0) planes respectively (JCPDS card no. 00-153-2069. The present (Zr-Co) NEG alloys are evaluated considering the FWHM of the most intense diffraction peak (1 0 0)values of inter planer spacing(d)= 3.985(Å), lattice constant (a)= a=6.903 (Å), FWHM=0.235θ, and crystalline sizeof Zr-Co series getter materials is D=34.422nm.

The XRD pattern of (Zr-Co-RE) getters at different concentrations of RE in Fig. 2. The (Zr-Co-RE) series is observed to contain 11 major fingerprint peaks at (0 0 2), (1 1 0), (0 4 0), (1 1 2), (1 3 1), (0 2 4), (1 3 3), (0 2 5), (2 2 2), (0 8 0) and (1 7 3). The observed h, k, l values are legibly identified with JCPDS Card No # 00-152-4752. It is interesting to note that five strong peaks were found around 2θ = 34.17°, 38.47°, 43.71°, 53.97°and 75.94°. These are corroborated with the earlier investigations[13,14]. The orthorhombic structure Zr_3Co, which has a stronger activation condition, is a base-centered orthorhombic lattice system that permits to translate into one of the base planes and the related space group (63. Cmcm). The values of these peaks corresponding Bragg angles and the lattice parameter (a) are calculated by using Unit Cell software. By using Debye-Scherrer's equation the crystallite sizes of the present (Zr-Co-RE) NEG alloys are evaluated considering the FWHM of the most intense diffraction peak (1 1 2)[15]. At higher temperatures, the crystalline size increases with increasing Zr concentration. The values of d-spacing and peak intensities increase as a function of Zr concentration. The FWHM is found to decrease with the reduction of Co concentration.

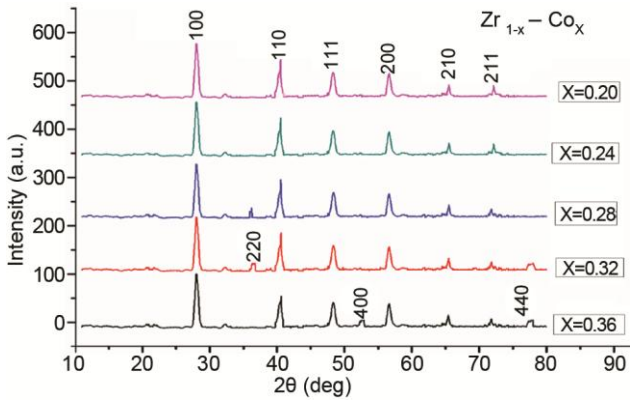

Fig. 1 — XRD patterns of (Zr-Co) series alloys.

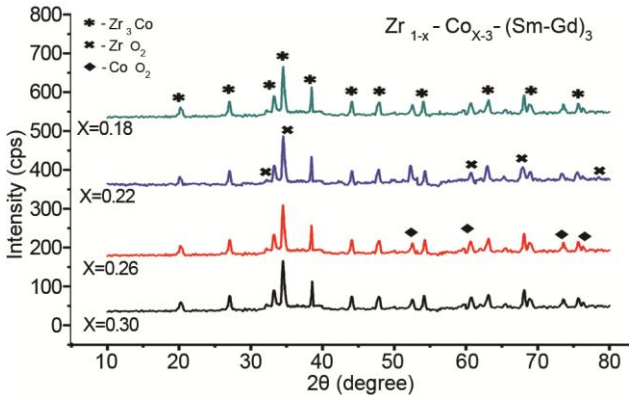

Fig. 2 — XRD patterns of ($Zr_{(1-x)}$-$Co_{(x-3)}$ -RE_3) series alloys.

The standard average lattice parameters of the orthorhombic crystal structure are a=3.43Å, b=10.85Å and c=8.78Å. Also, the volume is 317.25Å^3. This significantly enhances the absorption capacity of these alloys. Other small diffraction peaks of ZrO_2 phases of the orthorhombic structure are observed at 2θ=33.84^o, 35.12^o, 61.29^o, 68.38^o and 78.94^{o}corresponding to (0 2 0), (0 0 2), (3 1 1), (1 2 3) and (3 3 0) peaks with JCPDS card no. 00-154-5065. One moreminute diffraction peak of the CoO_2 phase, which has orthorhombic structure also observed at 2θ=52.85^o, 61.05^o, 75.42^o, and 77.19^o correlated to (2 0 9), (2 0 11), (0 2 8) and (2 0 15) peakswith JCPDS: 00-152-6822. This shows the property or behavior relating to sorption profile of these alloys[16-18].

The present (Zr-Co-RE) NEG alloys are evaluated considering the FWHM of the most intense diffraction peak (1 0 0) values of 'd' spacing(d)= 4.401(Å), lattice constant (a)= a=3.401, b=10.91,c=8.68 (Å), full width at half maximum (FWHM)= 0.524θ, and crystalline size of Zr-Co-RE series getter materials is D=153.980nm.

3.2 Density and porosity analysis

The experimental arrangement for bulk (d_b) and X-ray (d_x) densities (gm/cm^3) lattice constant (Å) besides porosity (%) particle size (D), specific surface area (S), Dislocation (δ) and micro strain (ε) of the present NEG getter materials with different concentrations has been measured, the obtained with Zr_{1-x}-$Co_x$where x varies between x = 0.36 to 0.20 in different concentration of 0.04 and Zr_{1-x}-Co_{x-3}-$RE_3$where x concentration weights between x = 0.30 to 0.18 in steps of 0.04 values are presented in the Table 1 and 2 .From Tables, the lattice parameter increasing with decrease of x is the finding of this paper[19, 10]. Lattice parameter increases when there is occupation of the interstitial place thus relaxation of the bond occurs. Lattice constant of pure zirconium is 3.1 A 0. The particle size (D) depends upon the FWHM of the highest peak of the XRD spectrum. These are two different samples with different X-ray characteristics[20-22]. So, there should be comparison between the same series rather than others.

From Table 1 and 2 the lattice parameter increasing with decrease of x is the finding of this work. Lattice parameter increases when there is occupation of the interstitial place thus relaxation of the bond occurs. Lattice constant of pure titanium is 2.95 A 0 and of pure zirconium is 3.1 A 0. The particle size D depends upon the FWHM of the highest peak of the XRD spectrum. These are two different samples with different X-ray characteristics. So, there should be comparison between the same series rather than others. The Surface area is inversely proportional to the particle size. After addition of RE particle size increased so the surface area decreased[23]. The values

Table 1 — Variation of lattice constant 'a', X-ray (d_x) and bulk (d_b) densities (gm/cm^3)) porosity %, particle size (D), Specific Surface Area(S), Dislocation(δ) and Micro Strain(ε) of Ti_{1-x}-$Co_x$and Zr_{1-x}-$Co_x$where x varies in between x = 0.36 to 0.20 in steps of 0.04.

S. No	Zr(1-x)-Cox	Con (x)	Lattice Constant (a)(Å)	X-ray-Density (dx)	Bulk-Density (db)	Porosity %	D (nm)	Spe. Surf. Area (S)X10^{-3} per unit	Dislocation (δ)X10^{-3} (nm^{-2})	Micro Strain (ε)X10^{-3}
1		0.36	3.187	13.394	23.673	43.42	82.366	5.432	1.474	0.875
2		0.34	3.118	13.173	22.721	42.022	90.79	5.016	1.213	0.788
3		0.28	3.177	13.528	23.132	41.518	97.281	4.806	1.174	0.736
4		0.24	3.196	13.267	23.528	43.611	103.753	4.36	0.928	0.695
5		0.2	3.204	13.148	24.546	46.431	135.215	3.374	0.546	0.533

Table 2 — Variation of lattice constant 'a', X-ray (d_x) and bulk (d_b) densities (gm/cm^3)) porosity %, particle size (D), Specific Surface Area(S), Dislocation(δ) and Micro Strain(ε) of Ti_{1-x}-$Co_x$and Zr_{1-x}-$Co_x$where x varies in between x = 0.36 to 0.20 in steps of 0.04.

Sr. No	Zr(1-x)-Co(x-3) -RE3	Con (x)	Lattice Constant (a) (Å)	X-ray-Density (dx)	Bulk-Density (db)	Porosity %	D (nm)	Spe. Surf. Area (S)X $10^{-3\ per}$ unit	Dislocation (δ)X10^{-3} (nm^{-2})	Micro Strain (ε)X10^{-3}
1		0.3	a=3.40 b=10.91 c=8.682	17.316	35.626	51.24	140.28	2.471	0.508	0.084
2		0.26	a=3.45 b=10.55 c=8.79	17.424	36.314	52.018	144.86	2.37	0.476	0.080
3		0.22	a=3.39 b=11.00 c=8.86	17.812	35.662	50.053	141.47	2.381	0.499	0.082
4		0.18	a=3.52 b=10.972 c=8.8	18.161	36.513	5.261	145.57	2.269	0.471	0.075

of lattice parameter, density and porosity are found to show improvement than pure elements as a function of substituting rare earth elements (RE). This may be due to the enhanced compactness of particles in their binding resulting in a raised density of materials. This may be understood with the increase in molecular weight of the samples due to their composition causing to increase the substitution of rare earth elements. The irregularity within a crystal structure that contains an abrupt change in the arrangement of atoms (dislocation) and the degree of distortion present in the crystalline lattice (micro strain) also decreases with the RE substitution. With substitution of RE elements, the porosity of the NEG materials is increased. It enhances the residual gases absorption rate causing more applicability in vacuum generations[24, 25].

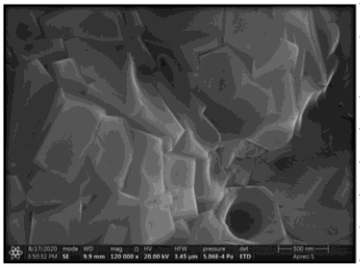

Zr-Co Series		
Element	Atomic wt%	Element wt%
CK	14.35	4.80
OK	15.16	15.71
Co K	28.88	30.73
Zr L	41.61	48.76
Total	100.00	100.00

Fig. 3 — Results of SEM micrograph and elemental concentration of (Zr-Co) NEG material.

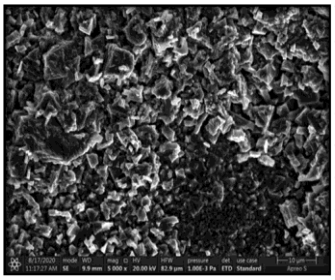

$Zr_{(1-x)}$-$Co_{(x-3)}$-RE_3		
Element	Atomic wt%	Element wt%
Ze L	81.14	73.66
Co L	16.64	24.02
Sm L	1.12	0.99
Gd L	1.09	1.32
Total	100.00	100.00

Fig. 4 — Results of SEM micrograph and elemental concentration of (Zr-Co-RE) NEG material.

3.3 Scanning electron microscope with EDS (EDX) study

The SEM images of pure Zr_{1-x}-Co_x where x varies between x = 0.36 to 0.20 in steps of 0.04 and Zr_{1-x}-Co_{x-3}-RE_3 where x concentration weight between x = 0.30 to 0.18 in steps of 0.04 shown in Fig. 3 & 4. In the Zr-based NEG specimens (Zr-Co), the bulk diffusion decreased with the rise of substituent concentration (x) may be due to causing reduced Zirconium content. The average particle size value appears to be diminishing as a function of x, and the computed particle size values agree with the crystallite size values obtained based on XRD measurements[26]. The observed porous structure on the surface of Zr-Co series nanostructure could reflect a higher capacity of gas absorption of this NEG materials nature. The structural stability of the (Zr-Co-RE) NEG materials are investigated by using EDS. Besides the free energy deposition of Zr, Co, and RE oxides, no other impurity peaks are exhibited in the spectra. As shown in Fig. 3 and 4 the most stable compounds are ZrO_2, and Co_2O_2. The obtained values of element weight % and atomic weight % for the series of Zr-Co and Zr-Co-RE are shown in the Fig. 3 & 4. The quantity of zirconium, cobalt, samarium, and gadolinium elements were found to be good as element weight %, atomic weight % and the results of EDS confirm the expected stoichiometry[27].

3.4 Transmissionelectron microscope study

Microstructure and related parameters such as average grain size and grain growth type, which determine the mechanical strength of materials, can be aided by morphological analysis. For RE substitution (Sm & Gd), the micrographs obtained of the Zr-Co shown in Fig. 5 and Zr-Co-RE shown in Fig. 6 series of NEG materials. The grain distribution in these photos Zr-Co (Series-1), Zr-Co-RE (Series-2) NEG series have average grain sizes and porosity nature calculated to displayed in Table 3.

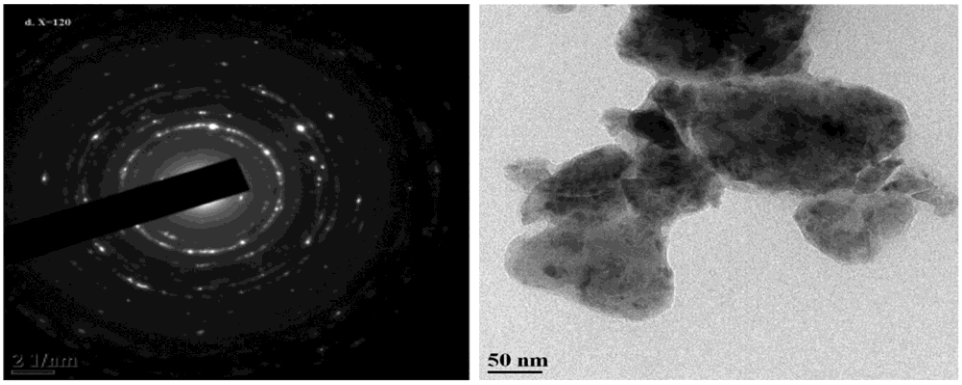

Fig. 5 — TEM images of (Zr-Co) (Series-1)

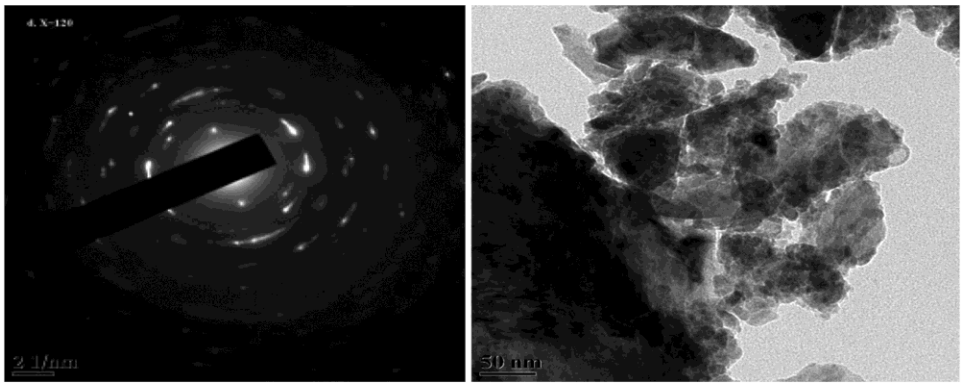

Fig. 6 — TEM images of (Zr-Co-RE) (Series-2)

Table 3 — Obtained the grain size (nm) of Zr_{1-x}-Co_x and Zr_{1-x}-Co_{x-3}-RE_3 series NEG materials.

S.no	Series-1 Zr_{1-x}-Co_x(nm)					Series-2 Zr_{1-x}-Co_{x-3}-RE_3 (nm)				
	Concentration (x)	Avg. Grain Size (nm)		Porosity (%)		Concentration (x)	Avg. Grain Size (nm)		Porosity (%)	
		SEM	TEM	SEM	TEM		SEM	TEM	SEM	TEM
1	0.36	34.23	0.36	44.65	46.17	0.30	129.82	135.76	52.43	56.34
2	0.32	36.19	0.32	38.43	44.76	0.26	152.90	159.12	55.87	54.76
3	0.28	41.64	0.28	45.87	41.31	0.22	162.79	173.25	58.12	57.19
4	0.24	37.75	0.24	48.81	42.14	0.18	148.43	162.31	53.98	54.03
5	0.20	32.56	0.20	43.27	45.54					

The TEM micrographs in the pictures show that the NEG materials effectively absorb residual gases in both cases. The fact that the two nano-sized series of rare earth substituted series improve the specific surface area and grain boundaries, allowing for fast gas diffusion, is remarkable. Because of the microstructure alteration, this could be an excellent way to increase the absorption rate of NEG materials[28]. The selected-area electron diffraction (SAED) patterns reflecting round circles at the middle point show that the grain sizes of the NEG samples lie in the nanocrystalline range. The obtained micrographs of pure Zr-Co and RE elements substituted and Zr-Co-RE series of NEG materials are indicating the enhanced values of average grain sizes and porosity for both the series relative to the RE elements non – substituted series (pure)[29, 30].

4 Conclusion

The effects of samarium and gadolinium (RE) in Ti-Co and Zr-Co non-evaporable getters are investigated in the present study, and the following conclusions are established.The non-evaporable getter materials (Zr-Co) and (Zr-Co-RE) were effectively synthesized at a temperature of 1000°C, and their structural properties and porosity nature were investigated.

a Based on the obtained XRD spectra, both series 1 (Zr-Co) are reflecting cubic crystalline structure containing point defects such as pores that spotted clearly among the crystal bonds. But the substitution of rare element, series 2 (Zr-Co-RE) exhibited cubic and orthorhombic crystalline structure. The substitution of rare earth element enhanced the bonding nature among molecules reflecting with very tight like a sponge, thus in contrast to the series 1 and2 series getter materials, the porosity behavior and mechanical strength of the materials has been modified largely. Crystalline size was found to increase with the substitution of RE element in both the series of materials relative to pure series of materials.

b With the rise of titanium concentration, the lattice constant and the size of the particle were also found to enhance their values. The same trend has been observed in the case of Zr-Co getter materials series too. The lattice constant increases from 3.18 to 3.20 Å (Zr-Co) series while for Zr-Co-RE series the attained values of lattice constant are a= 3.4 to 3.5, b= 10.91 to 10.97 and c= 8.68 to 8.81 Å.

c The getters need to contain maximized surface to volume ratios having high porosity facilitating to

adsorb gas molecules to be pumped into the internal areas of the getter materials. The present materials, i.e., the four series of materials found to show good mechanical characteristics, making these getter materials suitable for required conditions. A standard method for determination of the porosity and density of solid samples is adopted in the present studies. The obtained values of density and porosity of rare earth elements (RE) substituted materials are found to show improvement than the pure specimens.

d According to the XRD results in both series, when the cobalt content lowers, the FWHM reduces. Interatomic spacing, lattice parameter (a), volume of the cell (V), crystalline size (D), and Intensity(I) are all growing, and phase changes were shown in both series. When the lattice parameter is increased in both series, the NEG absorptionincerses more efficiently. The surface of the getter begins to pump more gases into the getter when these parameters are increased.

e The SEM with EDS study indicated that sintering at higher temperatures results in porous pellets with increased specific surface area and gas sorption capacity in both series. In addition, the EDS graphs revealed the getter material's optimal weight and atomic percentage.

f According to TEM microstructure investigations, the crystalline size of XRD patterns is proportional to the rise in particle size in a series; the histogram patterns can illustrate given above. The adsorption capacities of the non-evaporable getter materials increase as the activation temperature increases and porosity nature increases.

Acknowledgement

The authors gratefully acknowledge the support and facilities provided by the Department of Physics and Department of Chemistry, Centurion University of Management and Technology, Vizianagaram, Andhra Pradesh, India, for carrying out this research work. The authors also extend their sincere thanks to the Department of Nuclear Physics, Andhra University, Visakhapatnam, and the Department of Biotechnology and Bioinformatics, JSS Academy of Higher Education and Research (JSSAHER), Mysore, for their valuable support and collaboration.

References

1 Xu Y, Cui J, Cui H, Zhou H, Yang Z & Du J, J Alloys Compd, 661 (2016) 396.
2 Xiong Y H, Wei X Y, Qin G R, Yuan P, Mao C H & Du J, Vacuum, 82 (2008) 737.
3 Xu Y, Cui J, Cui H, Zhou H, Yang Z & Du J, J Electron Mater, 45 (2016) 386.
4 Zhang Y, Wei X Y, Mao C H, Li T F, Yuan P & Du J, J Alloys Compd, 485 (2009) 200.
5 Zhou H G, Wei X Y, Mao C H, Xiong Y H & Qin G R, Chin J Aeronaut, 20 (2007) 172.
6 Petti D, Cantoni M, Leone M, Bertacco R & Rizzi E, Appl Surf Sci, 256 (2010) 6291.
7 Zhou C, Li D, Zhou H, Liu X & Ma Z, Mater Res Express, 7 (2020) 036402.
8 Petti D, Cantoni M, Leone M, Bertacco R & Rizzi E, Appl Surf Sci, 256 (2010) 6291.
9 Zhang Y, Wei X Y, Mao C H, Li T F, Yuan P & Du J, J Alloys Compd, 485 (2009) 200.
10 Deng G, Zhao X, Wang S, Liu X, Li Z & Jiang L, Int J Hydrogen Energy, 38 (2013) 13050.
11 Zhou H G, Wei X Y, Mao C H, Xiong Y H & Qin G R, Chin J Aeronaut, 20 (2007) 172.
12 Moghadam A H, Dashtizad V, Kaflou A & Yoozbashizadeh H, Vacuum, 111 (2015) 9.
13 Moghadam A H, Dashtizad V, Kaflou A & Yoozbashizadeh H, Proc MEMA, (2015) 273.
14 Yoozbashizadeh H, Moghadam A H, Dashtizad V & Kaflou A, Int J Res Mater Sci, 1 (2015) 3.
15 Bu J G, Mao C H, Zhang Y, Wei X Y & Du J, J Alloys Compd, 529 (2012) 69.
16 Bandyopadhyay D, Sharma R C & Chakraborti N, J Phase Equilib, 21 (2000) 179.
17 Rostoker W, Trans Am Inst Min Metall Eng, 194 (1952).
18 Yu T H, Lin S J, Chao P & Huang C S, Acta Geol Sin, 2 (1974).
19 Phromma S, Wutikhun T, Kasamechonchung P, Eksangsri T & Sapcharoenkun C, Appl Sci, 10 (2020) 993.
20 Wu J, Microsc Microanal, 18 (2012) 1710.
21 Sato S, Kawabata A, Kondo D, Nihei M & Awano Y, Chem Phys Lett, 402 (2005) 149.
22 Straumal B B, Kilmametov A R, Ivanisenko Y, Mazilkin A A, Valiev R Z, Afonikova N S, Gornakova A S & Hahn H, J Alloys Compd, 735 (2018) 2281.
23 Behnajady M A &Eskandarloo H, Res ChemIntermed, 41 (2015) 2001.
24 Bamne J, Taiwade K, Sharma P K & Haque F Z, AIP Conf Proc, 2039 (2018) 020076.
25 Song H J, Han M K, Jeong H G, Lee Y T & Park Y J, Materials, 7 (2014) 3990.
26 26Kripyakevich P I, Burnashova V V & Markiv V Y, Dop Akad Nauk Ukr SSR, (1970).
27 Suyama R, Horiuchi H & Kume S, Yogyo Kyokai Shi, 95 (1987).
28 Lambert S, Leligny H & Grebille D, J Solid State Chem, 4 (2001).
29 Zhao Z, Wei X Y, Xiong Y H & Mao C H, Rare Metals, 28 (2009) 147.
30 Petti D, Cantoni M, Leone M, Bertacco R & Rizzi E, Appl Surf Sci, 256 (2010) 6291.